4-16-2021

# Direct Detection of 5-MeV Protons by Flexible Organic Thin-Film Devices

Ilaria Fratelli
*University of Bologna, Italy*

Andrea Ciavatti
*University of Bologna, Italy*

Enrico Zanazzi
*University of Trento, Italy*

Laura Basiricò
*University of Bologna, Italy*

Massimo Chiari
*INFN-Florence, Italy*

*See next page for additional authors*

# Direct Detection of 5-MeV Protons by Flexible Organic Thin-Film Devices

## Notes/Citation Information

## Authors

Ilaria Fratelli, Andrea Ciavatti, Enrico Zanazzi, Laura Basiricò, Massimo Chiari, Laura Fabbri, John E. Anthony, Alberto Quaranta, and Beatrice Fraboni

## APPLIED PHYSICS

# Direct detection of 5-MeV protons by flexible organic thin-film devices

Ilaria Fratelli[1,2]*, Andrea Ciavatti[1,2], Enrico Zanazzi[3,4], Laura Basiricò[1,2], Massimo Chiari[5], Laura Fabbri[1,2], John E. Anthony[6], Alberto Quaranta[3,4], Beatrice Fraboni[1,2]

The direct detection of 5-MeV protons by flexible organic detectors based on thin films is here demonstrated. The organic devices act as a solid-state detector, in which the energy released by the protons within the active layer of the sensor is converted into an electrical current. These sensors can quantitatively and reliably measure the dose of protons impinging on the sensor both in real time and in integration mode. This study shows how to detect and exploit the energy absorbed both by the organic semiconducting layer and by the plastic substrate, allowing to extrapolate information on the present and past irradiation of the detector. The measured sensitivity, $S = (5.15 \pm 0.13)$ pC Gy$^{-1}$, and limit of detection, LOD = $(30 \pm 6)$ cGy s$^{-1}$, of the here proposed detectors assess their efficacy and their potential as proton dosimeters in several fields of application, such as in medical proton therapy.

## INTRODUCTION

The development of detectors for protons and heavy particles is a long-lasting research topic not only for fundamental applications but also, more recently, for monitoring energy and flow of particles in ion beam applications. For instance, novel beam extraction technologies, like laser-driven accelerators, require fast and reliable systems for monitoring the beam quality (*1*). However, the most demanding application of ion beams, for which accurate measurements are increasingly needed, is hadron therapy of cancer. In this application field, ion beams, mostly proton beams, are used for the controlled treatment of cancer by focusing them onto small volumes to avoid the spreading of the radiation to healthy tissues (*2*). The effectiveness of the treatment is enhanced by tuning the beam both in intensity and in position to irradiate the tumor in a controlled way. For this reason, there is an increasing demand of systems optimized for the accurate recording and mapping of the dose delivered during a treatment plan (*3*). Besides this aspect, the next frontier for medical applications of proton beams is proton tomography, where high-energy (230 to 250 MeV) proton beams are used through the patient (*4*, *5*).

In proton therapy, a detector has to satisfy two major requirements. The first one is the capability to detect dose rate and position of the beam in real time. This is mandatory to have the control of the delivered dose if the beam position changes with respect to the patient. Because the needed accuracy for the beam position is about 1 mm, small involuntary movements, even due to respiration, can affect the treatment effectiveness (*6*). The second issue is the monitoring of the dose on healthy tissues. It is well known that the skin receives high doses during the irradiation treatment of various types of cancers (i.e., breast cancer), giving rise to long-term side effects (*7*). For instance, alopecia is a high risk in patients where brain tumors are treated with scanning proton beams (*8*). Another severe collateral effect involves the dose delivered to the rectal wall during prostate treatments, for

which dose monitoring methods with detectors inserted into rectal balloons have been studied (*9*, *10*). In all these cases, detectors have to be in contact with the patient to record the dose in real time.

A few types of detectors can reliably provide this information, but many are not suitable for the listed applications. For instance, dosimeters based on thermoluminescence, optical stimulated luminescence, and track measurements cannot be used for real-time monitoring. On the other side, calorimeters, ionization chambers, and gas detectors are very accurate but interfere with the beam parameters because they block the beam or are too bulky.

Suitable modern detectors are silicon-based MOSFET (metal oxide semiconductor field-effect transistor), silicon strips, and plastic scintillators. MOSFET detectors have been studied for the detection of the dose delivered both on skin and on rectal walls with good results (*9*, *11*). The main drawback is the need for accurate calibration procedures, because the detectors are intrinsically nonwater equivalent with an energy-dependent response. Moreover, MOSFET fabrication requires a clean room and high-level technology, and to date, no large-area detectors for imaging applications are in production. Last, the limited radiation hardness of MOSFETs leads to continuous tests for their reliability and to expensive substitution procedures.

Silicon microstrip detectors have been used for ion beam imaging with very good temporal and spatial resolution. However, high doses are required for a good image quality and noise can affect the analysis of the proton energy. More complex structures, like CMOS (complementary metal-oxide semiconductor) pixelated detectors, present low radiation hardness for daily use, together with the complexity of the readout procedure. Last, it has to be taken into account that all silicon-based detectors cannot be used for flexible systems adhering to the skin or to curved surfaces. An accurate review on the different detection methods has been realized by Seco *et al.* (*3*).

Plastic scintillators are also used for beam diagnostics. In particular, scintillating fibers are used for real-time dose delivery and beam imaging with very good results (*12*, *13*). Drawbacks for this approach are mainly related to the light detection, which has to be very sensitive to obtain reliable results. Therefore, photomultiplier tubes or silicon photomultipliers with a suitable readout chain have to be coupled to the fibers. Moreover, a dose calibration procedure requires accurate knowledge of the scintillation properties, namely, of the ionization

[1]Department of Physics and Astronomy, University of Bologna, Viale Berti Pichat 6/2, 40127 Bologna, Italy. [2]INFN-Bologna, Viale Berti Pichat 6/2, 40127 Bologna, Italy. [3]Department of Industrial Engineering, University of Trento, Via Sommarive 9, I-38123 Povo, Trento, Italy. [4]INFN-TIFPA, Via Sommarive 14, I-38123 Povo, Trento, Italy. [5]INFN-Florence, Via G. Sansone 1, 50019 Sesto Fiorentino, Florence, Italy. [6]Department of Chemistry and Center for Applied Energy Research, University of Kentucky, Lexington, KY 40506, USA.
*Corresponding author. Email: ilaria.fratelli2@unibo.it

quenching factor, and sometimes, the simultaneous detection with different scintillators is needed for achieving accurate measurements (14). Last, imaging with 1-mm resolution is a difficult task to obtain near the target, because arrays of fibers have to be assembled with a cumbersome setup. Moreover, the transmissivity of scintillating plastic fibers can be lowered by bending or mechanical stress due to the insertion in the setup or to the adjustment on the target, resulting in calibration errors.

To date, there is no example of organic semiconductor detectors used as proton beam dose monitoring systems. Organic semiconductors have been successfully used for the realization of efficient flexible x-ray dosimeters (15–20), and only few papers report a preliminary test with polymeric semiconducting sheets for the detection of α particles (20–23) and more recently for the detection of thermal neutrons (24).

Organic semiconductors have already been demonstrated to be reliable detectors for ionizing radiation, but they could offer also appealing properties for proton beam monitoring. They can be processed and deposited at low temperature (<150°C) by solution, leading the possibility to realize millimeter pixels of the order of mm$^2$ onto flexible and large-area substrates. Moreover, the facts that they do not require expensive fabrication setups and that they are reusable make them a potential low-cost, industrially scalable sensing system. Last, a crucial point for the dosimetry application is the fact that they are water tissue equivalent in terms of absorption and, consequently, the calibration of the sensor is not needed.

In this work, the first study on responsivity of organic semiconductor detectors to proton beams is presented. Both the real-time mode and the integration-mode response of the sensors are described, and the process of interaction between the charged particles and the active layer of the detector is discussed.

## RESULTS

The organic detectors we fabricated and tested are depicted in Fig. 1A. The devices have a photoconductor structure where the active semiconducting layer is an organic thin film (150 nm thick) of microcrystalline bis(triisopropylgermylethynyl)-pentacene (hereafter TIPGe-Pn), deposited by drop casting onto two interdigitated gold electrodes in coplanar architecture (Fig. 1A) (25). We deposited gold electrodes by thermal evaporation on a 125-μm-thick plastic substrate [i.e., polyethylene terephthalate (PET) or polyethylene naphthalate (PEN)], ensuring the mechanical flexibility of

the system. In particular, we fabricated and tested samples with the same channel length (i.e., the distance between the fingers of the electrodes) of $L = 30$ μm and two different width, i.e., $W = 205.5$ mm ($W/L = 6850$) and $W = 45$ mm ($W/L = 1500$).

TIPGe-Pn is an organic small molecule similar to bis(triisopropylsilylethynyl)-pentacene molecule (TIPS-Pn) by substituting the two silicon atoms with two germanium atoms (26, 27). The strong packing of the organic units and the oriented alignment of the microcrystalline structures (Fig. 1B) ensure efficient charge transport within the semiconducting layer. TIPGe-Pn–based detectors have been demonstrated to enhance the charge carrier mobility and the x-ray sensitivity with respect to TIPS-Pn–based counterparts (15, 28). All fabrication steps to implement these detectors are scalable to large-area, low-temperature (<180°C) compatible processes, thus allowing to obtain large-area, thin, and flexible detectors (Fig. 1C).

The detector response under proton irradiation was tested using a 5-MeV beam provided by the 3 MV Tandetron accelerator of the LABEC ion beam center (Laboratory of Nuclear Techniques for the Environment and Cultural Heritage, INFN Firenze, Italy). Proton beam currents used in this work are typically in the 1- to 100-pA range. The weak intensity of the beam is monitored and quantitatively measured using a rotating chopper (29), placed between the silicon nitride window and the sample, that intercepts the beam. Although the energy of ion therapy beams is commonly above 70 MeV, the proton energy tested in this work is of the order of the end-of-range values, in particular of the energies of scattered protons reaching internal healthy tissues surrounding the target.

Figure 2A depicts the entire experimental setup used to access the proton detection of the here reported sensing system. We enclosed the devices in a box, keeping the detector in the dark during the measurements, with a small aperture to let the proton beam in. We centered the sensor in front of the extracted proton beam (Fig. 2B). To determine the actual energy of the protons impinging onto the 150-nm-thick organic layer, the energy lost by the protons passing through the several layers interposed between the beam and the sensor (see Materials and Methods) has to be calculated. After passing through these layers, protons lose about 390 keV, as calculated with the stopping and range of ions in matter (SRIM) Monte Carlo code (30). Figure 2C reports the SRIM simulation of the linear energy transfer (LET) of each proton in the TIPGe film and in the PEN substrate. As can be observed, the total released energy, given by the integral of the curves, in the plastic substrate is much higher than
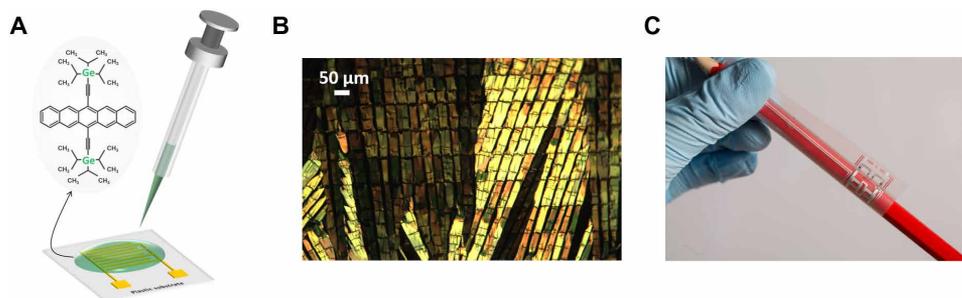


**Fig. 1. Organic thin film–based device: Architecture and morphology.** (**A**) Coplanar structure composed of two interdigitated electrodes (Au) deposited onto a plastic substrate (125 μm thick) by thermal evaporation. The organic semiconducting thin film is deposited on the top by drop casting, and it is composed of TIPGe-Pn. (**B**) Optical image of the well-aligned microcrystalline structures forming the thin-film semiconducting layer. (**C**) Flexibility of the here presented TIPGe-Pn–based detectors. Photo credit: Ilaria Fratelli, Department of Physics and Astronomy, University of Bologna, Italy.
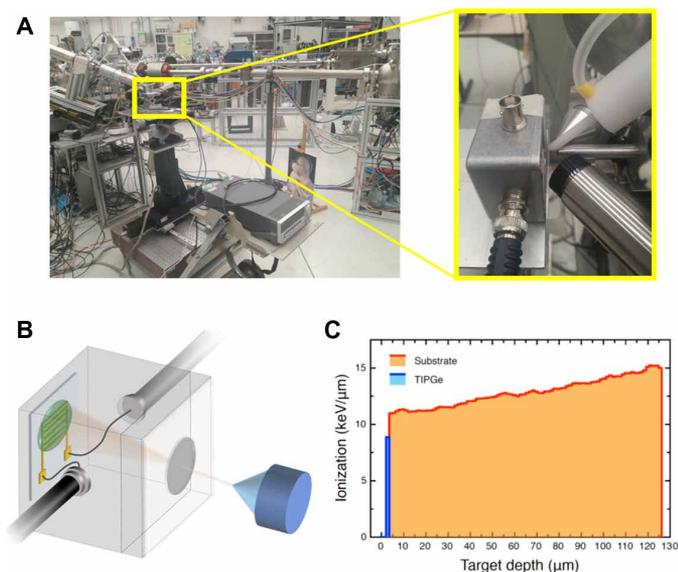
**Fig. 2. The 5-MeV proton irradiation setup.** (**A**) The detectors have been irradiated by 5-MeV protons at the LABEC center using an extracted beam line and tuning the fluences of protons in the range [$3.5 \times 10^9$ to $8.7 \times 10^{11}$] H$^+$ cm$^{-2}$. Photo credit: Ilaria Fratelli, Department of Physics and Astronomy, University of Bologna, Italy. (**B**) During the measurements, the devices were closed in a box, which keeps the organic detector in the dark. The protons passed through a 14-μm-thick Al window and 18 mm of air before impinging onto the active layer of the detector. (**C**) Simulated curve of the energy released by the proton beam in each layer.

the one deposited in the organic semiconductor due to the substantially different layer thicknesses. In particular, the energy lost by each proton within the TIPGe-Pn layer is, on average, 1.55 keV, while the energy absorbed by the plastic substrate is about 1590 keV. This difference can be effectively exploited to implement a proton detector able to simultaneously operate both in real-time mode (exploiting the absorption of the organic thin film) and in integration mode (based on the absorption within the plastic substrate), as detailed in the following.

During the irradiation, the sensors were polarized at low voltages (<1 V) to collect the charges generated by anelastic interactions of protons with the electrons of the semiconducting layer. The detector performance has been tested under consecutive ON/OFF cycles of exposure to 5-MeV proton beam, tuning the fluence of particles impinging onto the devices in the range between $3.5 \times 10^9$ H$^+$ cm$^{-2}$ and $8.7 \times 10^{11}$ H$^+$ cm$^{-2}$. The dynamic current response of the sensors is reported in Fig. 3 (A and B), where the colored areas of the graphs represent the time windows of proton irradiation. We carried out the measurements by either keeping the exposure time constant ($t = 10$ s; Fig. 3A) or varying it between 10 and 30 s (Fig. 3B).

Figure 3C zooms into one of the peaks reported in Fig. 3 (A and B), highlighting the typical curve of response to proton irradiation by the detector. The shadowed area indicates the total collected charges during the interval of exposure to the flux of protons. The small spikes during proton irradiation are due to the small metal plate of the chopper necessary for the accurate evaluation of the beam flux. As a result of the energy absorption from the impinging radiation, electron-hole pairs are generated within the organic semiconductor and the electrical current measured between the two electrodes increases by $\Delta I$. When the beam is switched off, the current has an initial fast drop due to the recombination of the charges, followed
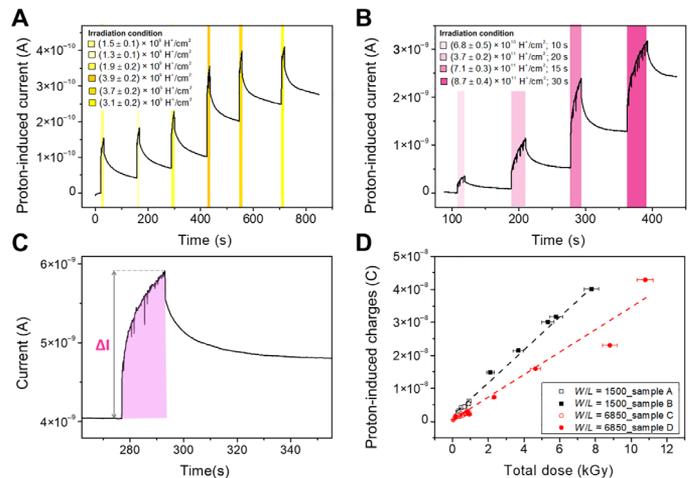


**Fig. 3. Real-time radiation detection response by organ semiconducting thin films.** (**A** and **B**) Current versus time response of the detectors irradiated by multiple ON/OFF cycles of protons tuning the incident fluences ($3.5 \times 10^9$ to $9 \times 10^{11}$ H$^+$ cm$^{-2}$). The detectors have been tested, keeping the exposure time constant $t = 10$ s (A) or varying it between 10 and 30 s (B). During the measurements, an electric field (applied bias <1 V) was imposed to the organic semiconducting layer. The time window of the irradiation is colored in the graphs, and the color intensity of the boxes indicates the intensity of the proton beam. (**C**) Highlight of dynamic response of the detector. The slow increase of the current indicates photoconductive gain effect. The current ($\Delta I$) is calculated as the difference between maximum peak current and the baseline current before the irradiation. The integral of the plot (colored in pink) represents the total charge induced by the protons. (**D**) Plots of the collected charges in function of the total dose of protons for two different $W/L$. The black squares correspond to $W/L = 1500$, while the red circles represent $W/L = 6850$. In both cases, the graphs indicate a linear response of the detector in a wide range of fluences (40 Gy to $11 \times 10^3$ Gy).

by a slower decay. The dynamic of the induced current peak is a fingerprint for the detection of ionizing radiation by thin-film organic semiconductor-based sensors. As recently discussed (*31, 32*), the current induced in organic thin film following exposure to ionizing radiation is increased by an inner mechanism of amplification [i.e., the photoconductive gain effect (*31*)] mediated by trap states. In particular, for p-type semiconductor such as TIPGe-Pn, due to the presence of electron traps, the negative charges are suddenly trapped within the organic thin film, and to maintain the charge neutrality, additional holes are continuously injected inside the channel of the device, so each radiation-induced charge contributes more than one time to the total current. Thus, the current increase $\Delta I$ corresponds to the induced hole current amplified by a gain factor $G$, defined as the ratio between the recombination time ($\tau_r$) of the trapped electrons and the transit time ($\tau_t$) of the holes through the channel. These two characteristic times are described by Eqs. 1 and 2

$$\tau_t = \frac{L^2}{\mu V} \quad (1)$$

$$\tau_r = \frac{\alpha}{\gamma} \left[ \alpha \cdot ln\left(\frac{\rho_0}{\rho_X}\right) \right]^{\frac{1-\gamma}{\gamma}} \quad (2)$$

where $L$ is the length of the channel, $\mu$ is the charge carrier mobility, $V$ is the applied voltage, $\alpha$ is the time scale of the trap states, $\gamma$ is related to the distribution of the trap states, and $\rho_0$ and $\rho_X$ are the intrinsic and radiation-induced charge densities of the organic

layer, respectively. These two characteristic times univocally describe the "rise" and "fall" shapes of the dynamic response of the sensor because they are intrinsically related to transport properties and to the density and energy distribution of the active traps, which determine the "real-time" detection process. According to this model, the proton-induced current can reach a saturation regime if the sensor is irradiated for a time, which exceeds a certain threshold voltage. In this case, a dynamic equilibrium between the generation and trapping of minority carriers and their recombination is reached, resulting in a plateau in proton-induced current during the exposure (see fig. S1).

Figure 3C shows how, after each exposure, the current does not return to the initial value, but it maintains an offset that depends on the absorbed total irradiation dose.

For each exposure cycle, the radiation dose absorbed by the sensor has been calculated by

$$D = \frac{E_{abs} \times N_{prot}}{\rho_{TIPG-Pn} \times Volume} \tag{3}$$

where $E_{abs}$ is the simulated value of the energy released by each proton into the organic thin film obtained by multiplying the organic layer thickness and the LET value extracted from the SRIM simulation reported in Fig. 2C, $N_{prot}$ is the number of protons impinging onto the sensor and monitored by the rotating beam chopper described in Materials and Methods, $\rho_{TIPG-Pn}$ is the density of the organic layer formed by TIPGe-Pn molecules (1.233 g cm$^{-3}$), and Volume is the active volume of the sensor, which has been calculated as the product of the organic layer thickness and the proton beam spot area that was centered and totally included onto the area of the sensor. We calculated the proton-induced charges collected during each exposure cycle as the integral of the induced current peaks (i.e., the colored shadow in Fig. 3C). Figure 3D reports the collected charges as a function of the total proton dose for four samples: two samples with $W/L$ = 1500 (black dots) and two samples with $W/L$ = 6850 (red dots). The response of all tested detectors is linear with increasing radiation dose in a wide range of doses between 40 Gy and 11 kGy. Different samples with equal geometry lay on the same fit line, assessing the reproducibility and the repeatability of the detection response. From the plots in Fig. 3D, we extracted the sensitivity of the detector (i.e., the induced charges collected per unit of absorbed dose) as the slope of the linear fitting curve, reaching the values of $S_{W/L=1500}$ = (5.15 ± 0.13) pC Gy$^{-1}$ and $S_{W/L=6850}$ = (3.40 ± 0.18) pC Gy$^{-1}$. The different responses achieved with the two geometries can be ascribed to the different electrical efficiency for the extraction/injection of the induced charges by the electrodes.

An important figure of merit for a detector is the minimum detectable dose, often indicated as limit of detection (LOD), that allows to envisage the potential exploitation of the detector for different applications. We calculated the LOD of the here presented sensors using the following equation

$$LOD = \frac{3 \times RMS_{signal}}{Sensitivity} \tag{4}$$

where $RMS_{signal}$ is the root mean square of the current flowing in the device in dark condition and Sensitivity is the higher sensitivity obtained. By applying this definition, a LOD down to (30 ± 6) cGy s$^{-1}$ has been estimated.

The linearity of the real-time response holds even after 28.5 kGy of proton irradiation, assessing the reliability and the radiation hardness of TIPGe-Pn–based detectors.

It is also noteworthy that, exploiting the inner amplification provided by the photoconductive gain mechanism, we can operate the detector at very low bias if compared with the typical voltages used for semiconductor nuclear detectors (i.e., tens/hundreds of volts). We choose low-bias operations as the best trade-off for this class of sensors for three different reasons. First, organic materials suffer from bias stress even at a few bias volts (33) (see fig. S2), and working at low voltages can improve the reliability and the stability of the sensor. Second, the low bias and the interdigitated architecture increase the signal-to-noise ratio of the detectors. Last, under the application point of view, this is a key aspect to achieve portable, light-weight, low-cost, even wearable technologies.

Up to now, we discussed the sensor's detection mechanism in real-time mode, based on the interaction between the proton beam and the organic thin film. However, the persistent current turns to be reproducible and scales with the total absorbed dose. Hereafter, we discuss how to exploit the gradual baseline shift induced by multiple successive exposures, to implement an integration-mode operation, following the irradiation history of the sensor.

Figure 4A reports the current-voltage characteristics (*I-V*) of a TIPGe-Pn detector before and after proton irradiation, and after up to 3 months of storage in the dark. The increase of conductivity of the organic layer due to the interaction with the proton beam is evident. The conductivity raises from (1.93 ± 0.08) × 10$^{-6}$ S m$^{-1}$ to (36.4 ± 0.1) × 10$^{-6}$ S m$^{-1}$ after 66 nC of incident protons. The effect is reversible, and despite the long relaxation time, full recovery occurs after 3 months [conductivity of (1.88 ± 0.07) × 10$^{-6}$ S m$^{-1}$]. Looking closely at the typical dynamic response curve of the detector to proton irradiation (see Fig. 4B), the total proton irradiation–induced current can be considered composed of two different contributions. The first one is the real-time response as a result of energy released in the organic semiconductor layer and photoconductive gain effect. This has already been discussed before and called $\Delta I$. The second contribution, here denoted as $I_0$, represents the current baseline shift due to the fixed charges trapped in the plastic substrate after each proton beam exposure and depends on the irradiation history of the detector. In analogy to the procedure described above, we calculated the total induced charges (i.e., the integral of the green area highlighted in the dynamic curve of Fig. 4B) and the dose corresponding to each exposure (Fig. 4C). The integrated amount of charges generated in the substrate, responsible for the current baseline shift (and of its long relaxation time), is linearly dependent on the integrated dose of proton irradiation received by the detectors. From the linear fit of the curve reported in Fig. 4C, the sensitivity of the detector, here thus operating in an integration mode, results $S$ = (6.97 ± 0.18) × 10$^{-1}$ pC Gy$^{-1}$. The generation of charges in polymeric foils following proton irradiation is an effect known in the literature (34–38) and is well justified in the here presented devices, fabricated onto a 125-µm-thick plastic substrate absorbing a consistent fraction of the proton energy (about 1590 keV per H$^+$; Fig. 2C).

We suggest that these proton-induced charges, accumulated in the plastic substrate (Fig. 4D), act as a bottom-gate effect for the organic semiconductor layer, increasing its electrical conductivity. This effect can be assimilated to what occurs in a field effect transistor (Fig. 4E), where the gate electrode is used to tune the density of
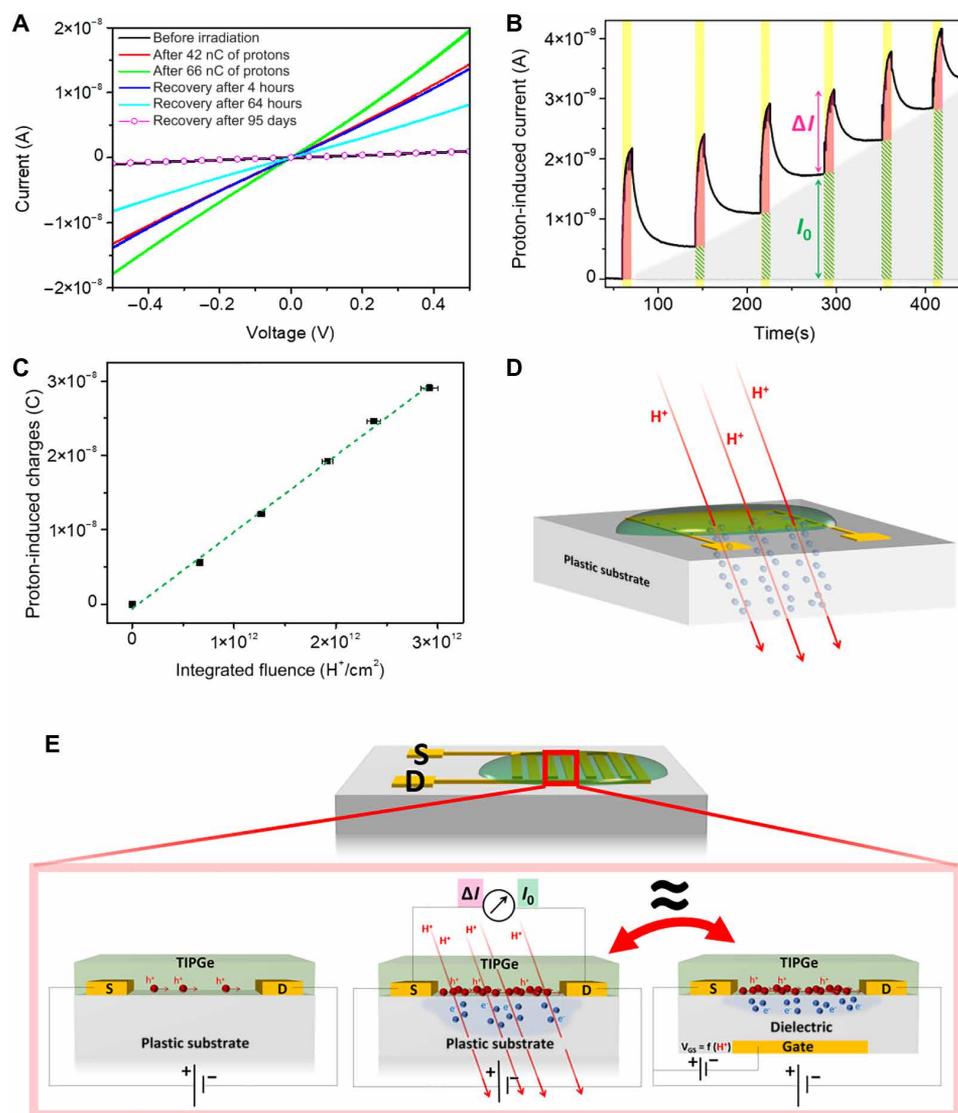
**Fig. 4. Organic proton sensor operated in integration mode.** (**A**) Current-voltage curves acquired before (black) the irradiation, after $2.5 \times 10^{11}$ incident protons (42 nC, red line), after $4 \times 10^{11}$ incident protons (66 nC, green line), and after 4 hours (blue line), 64 hours (light blue line), and 95 days (pink line and dots) of storage in the dark. The graph shows the increase of conductivity of the organic semiconducting layer due to the irradiation. (**B**) Dynamic curve (black line) of the current response of the detector to different fluences of incident protons [($4.5 \times 10^{-11}$ to $6.6 \times 10^{-11}$) H$^+$ cm$^{-2}$]. Two different contributions can be distinguished: $\Delta I$ (pink shadow) is the real-time response proportional to the dose (already described in Fig. 3), while $I_0$ (green shadow) represents the baseline shift due to the fixed charges trapped in the plastic substrate. (**C**) Linear increase of the total charge generated in the plastic substrate as a function of the integrated dose, which irradiates the sample. (**D** and **E**) Schematics of the detector integration-mode operation: the protons irradiating the sample generate charges in the polymeric foil with a very long relaxation time. These trapped negative charges induce an increase of the semiconductor conductivity, leading to higher source-drain current in the organic thin film. This effect is similar to what happens in an organic field effect transistor (OFET) structure, where the gate electrode is typically used to tune the current flowing between the source and drain electrodes. In this case, the irradiated polymeric substrate of the sensor acts as the bottom-gate electrode of an OFET structure, creating a gating effect proportional to the integrated dose of irradiating protons.

charges flowing in the thin channel at the semiconductor/dielectric interface, between the source and drain electrodes. Here, as the charges induced in the plastic substrate have a long lifetime (as assessed by the *I-V* curves; Fig. 4A), this gating effect adds up after each proton exposure, with a contribution proportional to the actual dose received, thus allowing to quantitatively monitor the irradiation history of the detector.

It is noteworthy that to collect and to exploit the information accumulated within the plastic substrate, the organic semiconducting

layer and its interface with the substrate play an essential role, as they permit to transduce into a source-drain current the information stored in the static charges induced in the substrate by proton irradiation. While the organic devices on PEN foils show the integrative response that we described above, similar devices with organic layer deposited onto Corning glass slides do not follow the same behavior. Only the sensors on PEN present the "memory" effect, while for devices onto glass, the proton irradiation induces a nonlinear decrease of the current and does not allow to extract any

information (fig. S3). This measurement confirms the crucial role of both the organic material and the substrate in the integrative response of the detector. In fact, proton irradiation effects and charge generation are less pronounced in glass (*35*).

We demonstrated the complete decoupling of the real-time detection response attributed to the organic semiconducting layer (and ruled by the photoconductive gain mechanism) from the integrative contribution due to the absorption of energy in the PEN substrate. The independence of these two distinct mechanisms of detection is demonstrated by the linearity of the generated charges and the total dose represented in Fig. 3D. Moreover, when considering any two real-time peaks obtained under the same proton fluence, they exactly overlap, demonstrating that, despite the different amount of charges induced in the substrate due to the different "history" of the detector, the organic semiconductor equally responds to the same fluence of protons. The two signals can thus be both reliably and effectively exploited to monitor the proton doses in an independent way (more details are shown in fig. S4).

## DISCUSSION

In conclusion, this study illustrates the direct detection of 5-MeV protons by organic thin-film devices realized on a plastic flexible substrate. The best sensitivity obtained by this new class of detectors is $S = (5.15 \pm 0.13)$ pC Gy$^{-1}$, and a LOD down to $(30 \pm 6)$ cGy s$^{-1}$ has been calculated. The sensors demonstrate a stable and reproducible response to proton beams in a range of fluences between $3.5 \times 10^9$ H$^+$ cm$^{-2}$ and $8.7 \times 10^{11}$ H$^+$ cm$^{-2}$ and maintain a linear response up to a total dose of 28.5 kGy. By exploiting the structure of this sensor, two different operation modes can be effectively used: (i) real-time mode sensing, where the amount of charges generated and collected at the electrodes is proportional to the released dose, and (ii) integration-mode sensing, where the energy released in the plastic substrate by the impinging protons generates static long life-time charges that accumulate in the polymeric substrate and induce an increase of conductivity in the semiconducting layer. To the best of our knowledge, this is the first study showing such a behavior in an organic device, demonstrating the potentiality of this new class of materials as flexible, portable, and human-tissue equivalent proton detectors.

## MATERIALS AND METHODS
### Device fabrication
Devices are fabricated onto a 125-μm-thick plastic foil (i.e., PET or PEN). The active layer of the device is formed by 150-nm-thick microcrystalline TIPGe-Pn (i.e. bis(triisopropylgermylethynyl)-pentacene). This organic small-molecule semiconductor is deposited from solution (i.e., 0.5 weight % in toluene) by drop casting onto two gold interdigitated electrodes. The devices are annealed at 90°C for 1 hour. The gold interdigitated electrodes are deposited by thermal evaporation and patterned by photolithography. The channel length is $L = 30\,\mu m$, while the channel width is, in one case, $W = 205.5$ mm ($W/L = 6850$) and, in the other, $W = 45$ mm ($W/L = 1500$).

### Proton irradiation
We irradiated the detectors using a 5-MeV beam provided by the 3 MV Tandetron accelerator of the LABEC ion beam center (INFN Firenze, Italy). The beam is extracted into ambient pressure through a 200-nm-thick Si$_3$N$_4$ membrane; the sample is typically installed at a distance of 8 mm from the extraction window. Proton beam currents used in this work are typically in the 1- to 100-pA range. The weak intensity of the extracted beam is monitored and quantitatively measured using a rotating chopper, placed between the silicon nitride window and the sample, that intercepts the beam; the chopper is a graphite vane covered with a thin nickel evaporation, and the Ni x-ray yield is used as an indirect measurement of the beam current (*29*).

To determine the actual energy of the protons impinging onto the 150-nm-thick organic layer, the energy lost by the protons passing through the several layers interposed between the beam and the sensor, namely, 200 nm of Si$_3$N$_4$ for the beam extraction window, 8 mm of mixed air-He (50%-50%) atmosphere in the gap between the extraction window and the metal box, 14 μm of Al for the entrance window of the box, where the sensor was enclosed, and 14 mm of air inside the box, has to be calculated. After passing through these layers, protons lose about 390 keV, as calculated with the SRIM Monte Carlo code (*30*).

## REFERENCES AND NOTES

1. M. Wu, J. Zhu, D. Li, T. Yang, Q. Liao, Y. Geng, X. Xu, C. Li, Y. Shou, Y. Zhao, Y. Lu, H. Lu, W. Ma, C. Lin, K. Zhu, X. Yan, Collection and focusing of laser accelerated proton beam by an electromagnetic quadrupole triplet lens. *Nucl. Instrum. Methods Phys. Res. Sect. A* **955**, 163249 (2020).

2. M. Durante, J. S. Loeffler, Charged particles in radiation oncology. *Nat. Rev. Clin. Oncol.* **7**, 37–43 (2010).

3. J. Seco, B. Clasie, M. Partridge, Review on the characteristics of radiation detectors for dosimetry and imaging. *Phys. Med. Biol.* **59**, R303–R347 (2014).

4. R. P. Johnson, Review of medical radiography and tomography with proton beams. *Rep. Prog. Phys.* **81**, 016701 (2018).

5. J. Ptacek, D. Locke, R. Finck, M. E. Cvijic, Z. Li, J. G. Tarolli, M. Aksoy, Y. Sigal, Y. Zhang, M. Newgren, J. Finn, Multiplexed ion beam imaging (MIBI) for characterization of the tumor microenvironment across tumor types. *Lab. Invest.* **100**, 1111–1123 (2020).

6. C. Bert, M. Durante, Motion in radiotherapy: Particle therapy. *Phys. Med. Biol.* **56**, R113 (2011).

7. M. Gieringer, J. Gosepath, R. Naim, Radiotherapy and wound healing: Principles, management and prospects (review). *Oncol. Rep.* **26**, 299–307 (2011).

8. G. Palma, A. Taffelli, F. Fellin, V. D'Avino, D. Scartoni, F. Tommasino, E. Scifoni, M. Durante, M. Amichetti, M. Schwarz, D. Amelio, L. Cella, Modelling the risk of radiation induced alopecia in brain tumor patients treated with scanned proton beams. *Radiother. Oncol.* **144**, 127–134 (2020).

9. K. Legge, P. B. Greer, D. J. O'Connor, L. Wilton, M. Richardson, P. Hunter, A. Wilfert, J. Martin, A. Rosenfeld, D. Cutajar, Real-time in vivo rectal wall dosimetry using MOSkin detectors during linac based stereotactic radiotherapy with rectal displacement. *Radiat. Oncol.* **12**, 41 (2017).

10. N. Hardcastle, D. L. Cutajar, P. E. Metcalfe, M. L. F. Lerch, V. L. Perevertaylo, W. A. Tomé, A. B. Rosenfeld, In vivo real-time rectal wall dosimetry for prostate radiotherapy. *Phys. Med. Biol.* **55**, 3859–3871 (2010).

11. I. S. Kwan, A. B. Rosenfeld, Z. Y. Qi, D. Wilkinson, M. L. F. Lerch, D. L. Cutajar, M. Safavi-Naeni, M. Butson, J. A. Bucci, Y. Chin, V. L. Perevertaylo, Skin dosimetry with new MOSFET detectors. *Radiat. Meas.* **43**, 929–932 (2008).

12. L. Archambault, T. M. Briere, F. Pönisch, L. Beaulieu, D. A. Kuban, A. Lee, S. Beddar, Toward a real-time in vivo dosimetry system using plastic scintillation detectors. *Int. J. Radiat. Oncol. Biol. Phys.* **78**, 280–287 (2010).

13. J. L. Cantley, C.-W. Cheng, F. B. Jesseph, T. K. Podder, V. C. Colussi, B. J. Traughber, L. E. Ponsky, R. J. Ellis, Real-time in vivo dosimetry for SBRT prostate treatment using plastic scintillating dosimetry embedded in a rectal balloon: A case study. *J. Appl. Clin. Med. Phys.* **17**, 305–311 (2016).

14. F. Alsanea, F. Therriault-Proulx, G. Sawakuchi, S. Beddar, A real-time method to simultaneously measure linear energy transfer and dose for proton therapy using organic scintillators. *Med. Phys.* **45**, 1782–1789 (2018).

15. L. Basiricò, A. Ciavatti, I. Fratelli, D. Dreossi, G. Tromba, S. Lai, P. Cosseddu, A. Bonfiglio, F. Mariotti, C. Dalla Val, V. Bellucci, J. E. Anthony, B. Fraboni, Medical applications of tissue-equivalent, organic-based flexible direct X-ray detectors. *Front. Phys.* **8**, 13 (2020).

16. M. J. Griffith, S. Cottam, J. Stamenkovic, J. A. Posar, M. Petasecca, Printable organic semiconductors for radiation detection: From fundamentals to fabrication and functionality. *Front. Phys.* **8**, 22 (2020).

17. H. M. Thirimanne, K. D. G. I. Jayawardena, A. J. Parnell, R. M. I. Bandara, A. Karalasingam, S. Pani, J. E. Huerdler, D. G. Lidzey, S. F. Tedde, A. Nisbet, C. A. Mills, S. R. P. Silva, High sensitivity organic inorganic hybrid X-ray detectors with direct transduction and broadband response. *Nat. Commun.* **9**, 2926 (2018).

18. B. Fraboni, A. Ciavatti, F. Merlo, L. Pasquini, A. Cavallini, A. Quaranta, A. Bonfiglio, A. Fraleoni-Morgera, Organic semiconducting single crystals as next generation of low-cost, room-temperature electrical X-ray detectors. *Adv. Mater.* **24**, 2289–2293 (2012).

19. L. Basiricò, A. Ciavatti, B. Fraboni, Solution-grown organic and perovskite X-ray detectors: A new paradigm for the direct detection of ionizing radiation. *Adv. Mater. Technol.* **6**, 2000475 (2021).

20. D. Zhao, M. Xu, B. Xiao, B. Zhang, L. Yan, G. Zeng, A. Dubois, P. Sellin, W. Jie, Y. Xu, Purely organic 4HCB single crystals exhibiting high hole mobility for direct detection of ultralow-dose X-radiation. *J. Mater. Chem. A* **8**, 5217–5226 (2020).

21. P. Beckerle, H. Ströbele, Charged particle detection in organic semiconductors. *Nucl. Instrum. Methods Phys. Res. Sect. A* **449**, 302–310 (2000).

22. A. Ciavatti, P. J. Sellin, L. Basiricò, A. Fraleoni-Morgera, B. Fraboni, Charged-particle spectroscopy in organic semiconducting single crystals. *Appl. Phys. Lett.* **108**, 153301 (2016).

23. L. Carman, H. Paul Martinez, L. Voss, S. Hunter, P. Beck, N. Zaitseva, S. A. Payne, P. Irkhin, H. H. Choi, V. Podzorov, Solution-grown rubrene crystals as radiation detecting devices. *IEEE Trans. Nucl. Sci.* **64**, 781–788 (2017).

24. P. Chatzispyroglou, J. L. Keddie, P. J. Sellin, Boron-loaded polymeric sensor for the direct detection of thermal neutrons. *ACS Appl. Mater. Interfaces* **12**, 33050–33057 (2020).

25. D. M. Hunter, J. A. Rowlands, Differences between transient photoconductivity in a-Se sandwich(bulk) and co-planar(interface) structures. *J. Mater. Sci. Mater. Electron.* **31**, 9114–9125 (2020).

26. J. C. Sorli, Q. Ai, D. B. Granger, K. Gu, S. Parkin, K. Jarolimek, N. Telesz, J. E. Anthony, C. Risko, Y. L. Loo, Impact of atomistic substitution on thin-film structure and charge transport in a germanyl-ethynyl functionalized pentacene. *Chem. Mater.* **31**, 6615–6623 (2019).

27. H. Zhang, Y. Yao, M. M. Payne, J. E. Anthony, J. W. Brill, Thermal diffusivities of functionalized pentacene semiconductors. *Appl. Phys. Lett.* **105**, 073302 (2014).

28. A. Ciavatti, L. Basiricò, I. Fratelli, S. Lai, P. Cosseddu, A. Bonfiglio, J. E. Anthony, B. Fraboni, Boosting direct X-ray detection in organic thin films by small molecules tailoring. *Adv. Funct. Mater.* **29**, 1806119 (2019).

29. M. Chiari, A. Migliori, P. A. Mandoò, Measurement of low currents in an external beam set-up. *Nucl. Instrum. Methods Phys. Res. Sect. B* **188**, 162–165 (2002).

30. J. F. Ziegler, M. D. Ziegler, J. P. Biersack, SRIM—The stopping and range of ions in matter (2010). *Nucl. Instrum. Methods Phys. Res. Sect. B* **268**, 1818–1823 (2010).

31. L. Basiricò, A. Ciavatti, T. Cramer, P. Cosseddu, A. Bonfiglio, B. Fraboni, Direct X-ray photoconversion in flexible organic thin film devices operated below 1 V. *Nat. Commun.* **7**, 13063 (2016).

32. I. Temiño, L. Basiricò, I. Fratelli, A. Tamayo, A. Ciavatti, M. Mas-Torrent, B. Fraboni, Morphology and mobility as tools to control and unprecedentedly enhance X-ray sensitivity in organic thin-films. *Nat. Commun.* **11**, 2136 (2020).

33. S. Park, S. H. Kim, H. H. Choi, B. Kang, K. Cho, Recent advances in the bias stress stability of organic transistors. *Adv. Funct. Mater.* **30**, 1904590 (2020).

34. M. Saito, F. Nishiyama, K. Kobayashi, S. Nagata, K. Takahiro, Reduction of light elements loss in polymer foils during MeV-proton irradiation by application of an aluminum coating. *Nucl. Instrum. Methods Phys. Res. Sect. B* **268**, 2918–2922 (2010).

35. R. Mishra, S. P. Tripathy, D. Sinha, K. K. Dwivedi, S. Ghosh, D. T. Khathing, M. Müller, D. Fink, W. H. Chung, Optical and electrical properties of some electron and proton irradiated polymers. *Nucl. Instrum. Methods Phys. Res. Sect. B* **168**, 59–64 (2000).

36. J. Čermák, L. Mihai, D. Sporea, Y. Galagan, J. Fait, A. Artemenko, P. Štenclová, B. Rezek, M. Straticiuc, I. Burducea, Proton irradiation induced changes in glass and polyethylene terephthalate substrates for photovoltaic solar cells. *Sol. Energy Mater. Sol. Cells* **186**, 284–290 (2018).

37. E. H. Lee, Ion-beam modification of polymeric materials—Fundamental principles and applications. *Nucl. Instrum. Methods Phys. Res. Sect. B* **151**, 29–41 (1999).

38. N. L. Singh, N. Shah, C. F. Desai, K. P. Singh, S. K. Arora, Modification of polyethylene terephthalate by proton irradiation. *Radiat. Eff. Defects Solids* **159**, 475–482 (2004).

# Science Advances

## Direct detection of 5-MeV protons by flexible organic thin-film devices

Ilaria Fratelli, Andrea Ciavatti, Enrico Zanazzi, Laura Basiricò, Massimo Chiari, Laura Fabbri, John E. Anthony, Alberto Quaranta and Beatrice Fraboni

| | |
|---|---|
| **ARTICLE TOOLS** | http://advances.sciencemag.org/content/7/16/eabf4462 |
| **SUPPLEMENTARY MATERIALS** | http://advances.sciencemag.org/content/suppl/2021/04/12/7.16.eabf4462.DC1 |
| **REFERENCES** | This article cites 38 articles, 0 of which you can access for free http://advances.sciencemag.org/content/7/16/eabf4462#BIBL |
| **PERMISSIONS** | http://www.sciencemag.org/help/reprints-and-permissions |

Use of this article is subject to the Terms of Service